Wavelength-scale photonic-crystal laser formed by electron-beam-induced nano-block deposition

Min-Kyo Seo,[1,*] Ju-Hyung Kang,[1] Myung-Ki Kim,[1] Byeong-Hyeon Ahn,[1] Ju-Young Kim,[1] Kwang-Yong Jeong,[1] Hong-Gyu Park,[2] and Yong-Hee Lee[1]

[1]*Department of Physics, Korea Advanced Institute of Science and Technology, Daejeon 305-701, Korea*
[2]*Department of Physics, Korea University, Seoul 136-701, Korea*
[*]*Corresponding author: minkyo.seo@gmail.com*

Abstract: A wavelength-scale cavity is generated by printing a carbonaceous nano-block on a photonic-crystal waveguide. The nanometer-size carbonaceous block is grown at a pre-determined region by the electron-beam-induced deposition method. The wavelength-scale photonic-crystal cavity operates as a single mode laser, near 1550 nm with threshold of ~100 μW at room temperature. Finite-difference time-domain computations show that a high-quality-factor cavity mode is defined around the nano-block with resonant wavelength slightly longer than the dispersion-edge of the photonic-crystal waveguide. Measured near-field images exhibit photon distribution well-localized in the proximity of the printed nano-block. Linearly-polarized emission along the vertical direction is also observed.

OCIS codes: (230.5298) Photonic crystals; (220.4241) Nanostructure fabrication; (140.3945) Microcavities; (250.5300) Photonic integrated circuits.

References and links

1. O. Painter, R. K. Lee, A. Scherer, A. Yariv, J. D. O'Brien, P. D. Dapkus, and I. Kim, "Two-Dimensional Photonic Crystal Defect Laser," Science **284**, 1819-1821 (1999).
2. H.-G. Park, S.-H. Kim, S.-H. Kwon, Y.-G. Ju, J.-K. Yang, J.-H. Baek, S.-B. Kim, and Y.-H. Lee, "Electrically Driven Single-Cell Photonic Crystal Laser," Science **305**, 1444-1447 (2004).
3. S. Strauf, K. Hennessy, M. T. Rakher, Y. S. Choi, A. Badolato, L. C. Andreani, E. L. Hu, P. M. Petroff, and D. Bouwmeetster, "Self-Tuned Quantum Dot Gain in Photonic Crystal Lasers," Phys. Rev. Lett. **96**, 27404 (2006).
4. D. Englund, D. Fattal, E. Waks, G. Solomon, B. Zhang, T. Nakaoka, Y. Arakawa, Y. Yamamoto, and J. Vučković, "Controlling the Spontaneous Emission Rate of Single Quantum Dots in a Two-Dimensional Photonic Crystal," Phys. Rev. Lett. **95**, 013904 (2005).
5. K. Hennessy, A. Badolato, M. Winger, D. Gerace, M. Atatüre, S. Gulde, S. Fält, E. L. Hu, and A. Imamoğlu, "Quantum nature of a strongly coupled single quantum dot–cavity system," Nature **445**, 896-899 (2007).
6. D. Englund, A. Faraon, I. Fushman, N. Stoltz, P. Petroff, and J. Vučković, "Controlling cavity reflectivity with a single quantum dot," Nature **450**, 857-861 (2007).
7. M. Lončar, A. Scherer, and Y. Qui, "Photonic crystal laser sources for chemical detection," Appl. Phys. Lett. **82**, 4648-4650 (2003).
8. E. Chow, A. Grot, L. W. Mirkarimi, M. Sigalas, and G. Girolami, "Ultracompact biochemical sensor built with two-dimensional photonic crystal microcavity," Opt. Lett. **29**, 1093-1095 (2004).
9. S. Kita, K. Nozaki, and T. Baba, "Refractive index sensing utilizing a cw photonic crystal nanolaser and its array configuration," Opt. Express **16**, 8174-8180 (2008).
10. B. Maune, M. Loncar, J. Witzens, M. Hochberg, T. Baehr-Jones, D. Psaltis, A. Scherer, and Y. M. Qiu, "Liquid-crystal electric tuning of a photonic crystal laser," Appl. Phys. Lett. **85**, 360-362 (2004).
11. S. H. Kim, J. H. Choi, S. K. Lee, S. H. Kim, S. M. Yang, Y. H. Lee, C. Seassal, P. Regrency, and P. Viktorovitch, "Optofluidic integration of a photonic crystal nanolaser," Opt. Express **16**, 6515-6527 (2008).
12. J. D. Joannopoulos, R. D. Meade, and J. N. Winn, *Photonic crystals* (Princeton, New York, 1995).

#107040 - $15.00 USD Received 2 Feb 2009; revised 26 Mar 2009; accepted 6 Apr 2009; published 9 Apr 2009

13. Y. A. Vlasov, M. O'Boyle, H. F. Hamann and S. J. McNab, "Active control of slow light on a chip with photonic crystal waveguides," Nature **438**, 65-69 (2005).
14. K. Nozaki, H. Watanabe, and T. Baba, "Photonic crystal nanolasers monolithically integrated with passive waveguide for efficient light extraction," Appl. Phys. Lett. **92**, 021108 (2008).
15. K. Hennessy, A. Badolato, A. Tamboli, P. M. Petroff, E. L. Hu, M. Atatüre, J. Dreiser, and A. Imamoğlu, "Tuning photonic crystal nanocavity modes by wet chemical digital etching," Appl. Phys. Lett. **87**, 021108 (2005).
16. K. Hennessy, C. Högerle, E. L. Hu, A. Badolato, and A. Imamoğlu, "Tuning photonic nanocavities by atomic force microscope nano-oxidation," Appl. Phys. Lett. **89**, 041118 (2006).
17. R. Ferrini, J. Martz, L. Zuppiroli, B. Wild, V. Zabelin, L. A. Dunbar, R. Houdré, M. Mulot, and S. Anand, "Planar photonic crystals infiltrated with liquid crystals: optical characterization of molecule orientation," Opt. Lett. **31**, 1238 (2006).
18. A. Faraon, D. Englund, D. Bulla, B. Luther-Davies, B. J. Eggleton, N. Stoltz, P. Petroff, and J. Vučković, "Local tuning of photonic crystal cavities using chalcogenide glasses," Appl. Phys. Lett. **92**, 043123 (2008).
19. M.-K. Seo, H.-G. Park, J.-K. Yang, J.-Y. Kim, S.-H. Kim, and Y-H. Lee, "Controlled sub-nanometer tuning of photonic crystal resonator by carbonaceous nano-dots," Opt. Express **16**, 9829 (2008).
20. H.-G. Park, C. J. Barrelet, Y. Wu, B. Tian, F. Qian, and C. M. Lieber, "A wavelength-selective photonic-crystal waveguide coupled to a nanowire light source," Nature Photonics **2**, 622 (2008).
21. S. Gardin, F. Bordas, X. Letartre, C. Seassal, A. Rahmani, R. Bozio, P. Viktorovitch, "Microlasers based on effective index confined slow light modes in photonic crystal waveguides," Opt. Express **16**, 6331 (2008).
22. M.-K. Kim, I.-K. Hwang, M.-K. Seo, and Y.-H. Lee, "Reconfigurable microfiber-coupled photonic crystal resonator," Opt. Express **15**, 17241 (2007).
23. C. L. C. Smith, U. Bog, S. Tomljenovic-Hanic, M. W. Lee, D. K. C. Wu, L. O'Faolain, C. Monat, C. Grillet, T. F. Krauss, C. Karnutsch, R. C. McPhedran, B. J. Eggleton, "Reconfigurable microfluidic photonic crystal slab cavities," Opt. Express **16**, 15887 (2008).
24. B. S. Song, S. Noda, T. Asano, and Y. Akahane, "Ultra-high-Q photonic double-heterostructure nanocavity," Nature Materials **4**, 207 (2005).
25. S. Tomljenovic-Hanic, C. M. Sterke, M. J. Steel, B. J. Eggleton, Y. Tanaka and S. Noda, "High-Q cavities in multilayer photonic crystal slabs," Opt. Express **15**, 17248 (2007).
26. P. El-Kallassi, S. Balog, R. Houdré, L. Balet, L. Li, M. Francardi, A. Gerardino, A. Fiore, R. Ferrini, and L. Zuppiroli, "Local infiltration of planar photonic crystals with UV-curable polymers," J. Opt. Soc. Am. B **25**, 1562 (2008).
27. M. Kristian, N. M. Dorte, M. R. Anne, C. Anna, C. A. Charlotte, B. Michael, J. H. Claus, and B. Peter, "Solid Gold Nanostructures Fabricated by Electron Beam Deposition," Nano Lett. **3**, 1499 (2003).
28. N. Silvis-Cividjian, C. W. Hagen, P. Kruit, M. A. J. v.d. Stam, and H. B. Groen, "Direct fabrication of nanowires in an electron microscope," Appl. Phys. Lett. **82**, 3514 (2003).
29. M.-F. Yu, O. Lourie, M. J. Dyer, K. Moloni, T. F. Kelly, and R. S. Ruoff, "Strength and Breaking Mechanism of Multiwalled Carbon Nanotubes Under Tensile Load," Science **287**, 637 (2000).
30. S.-H. Kim, G.-H. Kim, S.-K. Kim, H.-G. Park, Y.-H. Lee, and S.-B. Kim, "Characteristics of a stick resonator in a two-dimensional photonic crystal slab," J. Appl. Phys. **95**, 411 (2004).
31. E. D. Palik, *Handbook of Optical Constants of Solids II* (Academic Press, San Diego, 1998).
32. We used the following equation to estimate the absorption loss of the CNB: $2\pi/(\lambda Q_{abs}) = 2\pi/\lambda\ (1/Q_m - 1/Q_t)$ [33], where $2\pi/(\lambda Q_{abs})$, λ, Q_m and Q_t are the absorption loss, resonant wavelength, measured and theoretical Q factor respectively. The effect of the fabrication imperfection is included in this estimated absorption loss.
33. M. Borselli, T. J. Johnson and O. Painter, "Beyond the Rayleigh scattering limit in high-Q silicon microdisks: theory and experiment," Opt. Express **13**, 1515-1530 (2005).
34. M. W. McCutcheon and M. Lončar, "Design of silicon nitride photonic crystal nanocavity with a quality factor of one million for coupling to a diamond crystal," Opt. Express **16**, 19136 (2008).

1. Introduction

High-quality (Q) photonic-crystal (PhC) cavities offer possibilities of low-threshold lasers [1-3], single photon sources [4], **q**uantum optical applications [5, 6], micro-fluidics and chemical detections [7-11] and optical integrated circuits [12-14]. These high-performance optical applications require precise spectral and spatial positioning of the PhC cavity. For the spectral tuning, various post-processing methods have been reported such as wet chemical digital etching [15], atomic force microscope (AFM) nano-oxidation [16], liquid crystal infusion [17], photosensitive tuning of chalcogenide glasses [18] and electron beam induced

#107040 - $15.00 USD Received 2 Feb 2009; revised 26 Mar 2009; accepted 6 Apr 2009; published 9 Apr 2009

carbonaceous nano-dot deposition [19]. On the other hand, the formation of a wavelength-scale cavity in a desired position still remains a challenge. The spatial overlap of the cavity resonant mode with the active material is particularly needed to control and maximize the interaction between the cavity mode and the active material [5, 20]. For example, placing a spectrally-right quantum dot at a spatially-right place of PhC cavity is critical for a practical single photon source.

Recent years PhC micro-cavities formed at a desired position have been reported, such as PhC cavities with a polymethyl methacrylate (PMMA) layer patterned onto a PhC waveguide [21] and reconfigurable PhC resonators using a tapered micro-fiber [22] or air-hole infiltration [23]. Both cavities are generated by changing the effective index in a PhC waveguide and constructing a photonic double-heterostructure [24, 25]. In the reconfigurable PhC cavities, the effective refractive index is changed by attaching the micro-fiber to a PhC waveguide or infiltrating PhC air-holes with fluid drawn by a tapered micro-tip. However, these reconfigurable PhC resonators also have certain limitations. Additional alignment procedure in electron-beam lithography is necessary to fabricate the PMMA PhC cavity. More recently, local photo-polymerization technique using acrylate monomers and a ultra-violet laser has been reported but the spatial resolution is inevitably limited by the wavelength of the UV laser [26]. In this study, we propose and demonstrate a wavelength-scale photonic-crystal cavity laser formed by direct printing of a carbonaceous nano-block (CNB) on a PhC waveguide, using electron-beam-induced deposition (EBID) method. This EBID method, which is performed just by electron beam scanning, enables us to form the wavelength-scale PhC cavity at the predetermined position with a nanometer-scale resolution and achieve the Q factor and emission output direction of the cavity mode adjusted to application purpose by changing the position and size of the CNB.

2. Printing an EBID nano-block on a PhC waveguide

The EBID technique based on scanning electron microscope (SEM) is a versatile tool that enables the construction of various nano-structures such as nano-tips [27], nanowires [28] and thin films. By injecting proper precursors into a SEM chamber, complicated three-dimensional (3D) nano-structures composed of dielectrics or metals can be generated [29]. Even without any precursor, carbonaceous nano-structures are grown from organic molecules of diffusion vacuum pump oil, as shown in Fig. 1(a). In particular, by scanning focused electron beams over a certain area repeatedly, carbonaceous nano-blocks (CNBs) can be formed (Fig. 1(b)). The size and the thickness of a CNB are controlled by the scanning area and deposition time, respectively. We used the SEM (Hitachi S-4300, field emission type) with an acceleration voltage of 5 kV and beam current of ~100 pA.

#107040 - $15.00 USD Received 2 Feb 2009; revised 26 Mar 2009; accepted 6 Apr 2009; published 9 Apr 2009

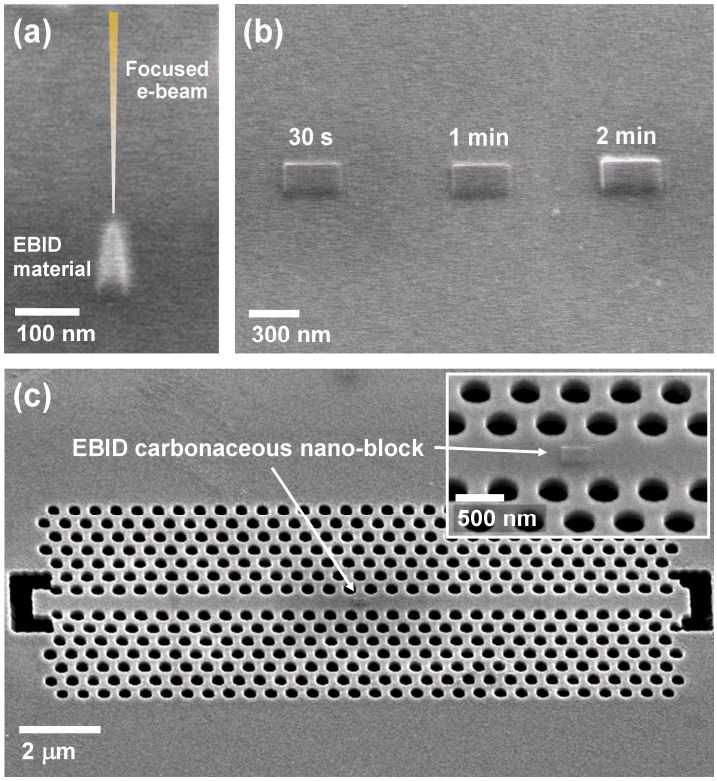

Fig. 1. (a) SEM image of an EBID carbonaceous nano-dot. (b) Three CNBs of different deposition times of 30, 60, and 120 seconds, respectively, taken at an angle of 45 degrees. (c) CNB printed on PhC waveguide.

We construct wavelength-scale cavities by printing a nano-block on a PhC slab waveguide. First, we fabricate a PhC slab waveguide using an InGaAsP single quantum well (SQW) slab structure grown by metal organic chemical vapor deposition (MOCVD). The InGaAsP SQW has a central emission peak of ~1550 nm and a spectral width of ~100 nm. In Fig. 1(c), the lattice constant, the radius of air hole and slab thickness of the PhC waveguide are ~520 nm, ~155 nm and ~210 nm, respectively. Two trenches with a horseshoe shape at both sides of the PhC waveguide are introduced to ease the etching of the InP sacrificial layer beneath the InGaAsP SQW slab. Finally a CNB is fabricated at the center of the PhC waveguide by EBID and generates a photonic potential well at the CNB position.

3. Theoretical investigation using finite-difference time-domain method

In order to understand the effects of the CNB printing, we compare dispersion characteristics of PhC waveguides with and without the CNB film, using 3D finite-difference time-domain (FDTD) methods with periodic boundary conditions. In triangular lattice PhC waveguides, two types of guided modes are allowed as shown in Fig. 2(a) [30]. We focus on the even-symmetry guided mode, because it has a small group velocity and thus is expected to interact with the active material strongly. In general, the dispersion curve red-shifts with the refractive index. Note that the deposition of a nano-block increases the effective index of the printed region and a CNB photonic double-heterostructure is constructed near the dispersion edge where $k_x a/2\pi = 0.5$ as shown in Figs. 2(a)-2(c). When we plot the cutoff frequency of the guided mode along the waveguide, a square photonic potential well can be drawn (Fig. 2(c)). A new CNB resonant mode can now be created in this potential well. In fact, the existence of

#107040 - $15.00 USD Received 2 Feb 2009; revised 26 Mar 2009; accepted 6 Apr 2009; published 9 Apr 2009

the CNB resonance is computationally confirmed at a frequency slightly below the cutoff of the even-symmetry guided mode. Those photons confined in this mode are not allowed to propagate along the PhC waveguides that sandwich the nano-block region. A calculated electric field intensity profile is shown in Fig. 2(b). As expected, photons are well confined in the CNB cavity.

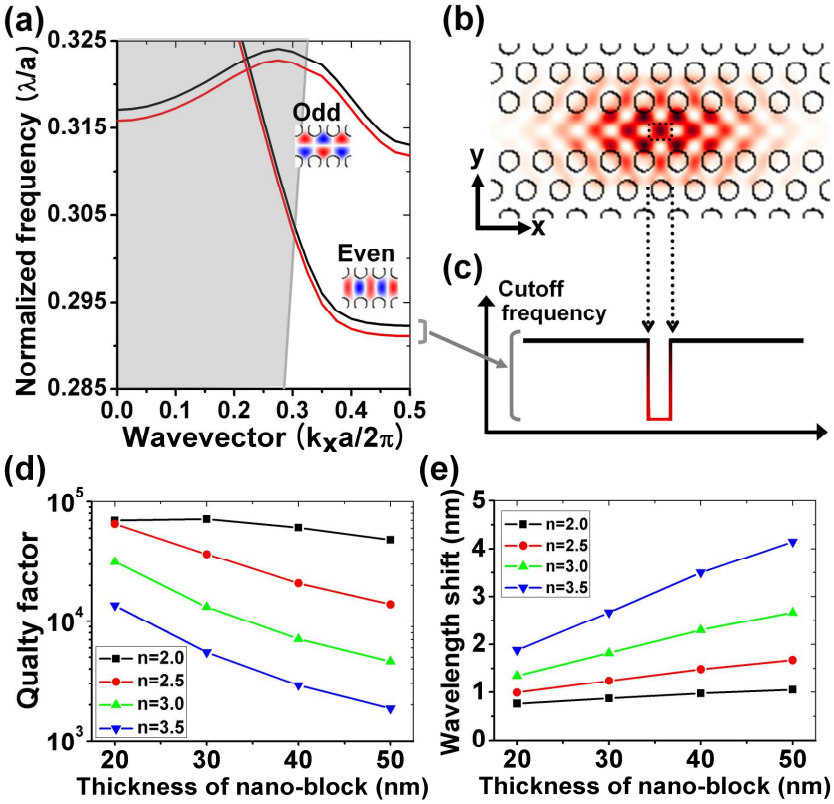

Fig. 2. (a) Dispersion of PhC waveguide. PhC lattice constant = a. Air hole radius = 0.30 a. Insets show H_z-profiles of the even- and odd-symmetry guided modes. (b) Calculated electric field intensity profile of the EBID PhC cavity mode. The refractive index and the thickness of the CNB are 3.0 and 40 nm, respectively. Contours of the PhC waveguide and the CNB are superimposed. (c) Plot of the cutoff frequency of the photonic double-heterostructure. Calculated Q factor (d) and cutoff wavelength-shift (e) with various thicknesses and refractive indices of the CNB, when the CNB is created above the electric field maximum of the slab.

Considering optical properties of amorphous hydrogenated carbon films [31] and previous data on CNBs [19], the index of the CNB is likely to lie between 2.0 and 3.5. Simulations employing a non-absorbing dielectric block are expected to estimate the upper bound of Q factor. Figures 2(d) and 2(e) show the calculated Q factor and cutoff wavelength-shift of the EBID PhC cavity plotted as a function of the thickness of the CNBs with different refractive indices. The wavelength shift is calculated by changing the refractive index and the thickness of the CNB from 20 nm to 50 nm by a step of 10 nm. The main source of losses is believed to be the scattering by the additional dielectric structure. We would like to lead the calculated results to the indirect estimation of Q factor from the cutoff shift. For example, in case when the thickness and refractive index of the CNB is 40 nm and 3.0 respectively, a cutoff wavelength shift of ~2.4 nm and a Q factor of ~7000 can be estimated from Figs. 2(d) and

#107040 - $15.00 USD Received 2 Feb 2009; revised 26 Mar 2009; accepted 6 Apr 2009; published 9 Apr 2009

2(e). However, even the slightest CNB absorption can bring forth serious problems and has to be taken into careful consideration, although the extinction coefficient of the carbonaceous material is known to be smaller than 10^{-2} near 1550 nm [31]. The calculated mode volume is ~1.4 $(\lambda/n)^3$ and found to decrease with the cutoff shift.

4. Experimental demonstration of the EBID PhC Laser

Near-field images of resonant modes can directly show optical features of wavelength-scale lasers and we take images of the fabricated EBID PhC laser using a 50x objective lens with a numerical aperture of 0.85 (Fig. 3(a)). The laser is pumped by 980-nm InGaAs laser diode (10-ns pulses, interval of 1 μs) at room temperature and the pumping laser is focused to a spot with a diameter of ~3 μm. Figure 3(a) exhibits photon confinement in the region of the CNB and 3(d) shows light emission into the vertical direction. The vertical emission from the CNB can be understood as follows: the CNB located above the electric field maximum of the slab (Fig. 2(c)) breaks the delicate balance of the field distribution and effectively generates a net electric dipole moment which can cause strong vertical emission. This observation agrees with the 3D FDTD simulation results of Figs. 3(c) and 3(d). The calculated vertical component of the propagating Poynting vector at a vertical position of 1.5 μm above the slab (Fig. 3(c)) compares well with the measured near-field profile. In addition, the vertical emission from the EBID PhC laser mode, as shown in Fig. 3(d), guarantees good coupling to conventional fiber optics through optical microscope lens.

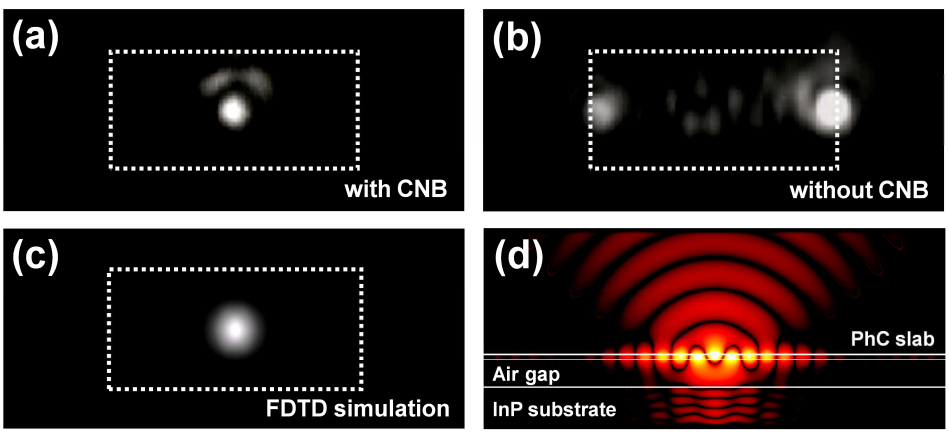

Fig. 3. Near-field images (a) of an EBID PhC laser with a CNB located above the electric field maximum at the center of the PhC waveguide, (b) of an even-symmetry dispersion-edge mode laser without CNB. The dotted rectangle indicates the boundary of the fabricated PhC pattern shown in Fig. 1(c). (c) Calculated vertical component of the Poynting vector by FDTD methods. (d) Side view of electric field intensity profile (log scale).

In comparison, we observed a lasing image of Fig. 3(b) from the identical PhC waveguide before the CNB printing. Note that this is completely different from Fig. 3(a). In Fig. 3(b), the even-symmetry dispersion-edge mode of the PhC waveguide is stimulated due to small group velocity and strong scattering is observed at the ends of the waveguide. The near-field measurements of the lasing modes in the PhC waveguide structures with and without the CNB demonstrate that lasing action is unambiguously achieved in the wavelength-scale CNB cavity.

To further investigate characteristics of the EBID PhC cavity mode, PL spectra are measured before and after printing a CNB on the identical PhC waveguide. In the original PhC waveguide without CNB, the even- and odd-symmetry guided modes are polarized in the

#107040 - $15.00 USD Received 2 Feb 2009; revised 26 Mar 2009; accepted 6 Apr 2009; published 9 Apr 2009

directions orthogonal and parallel to the PhC waveguide axis, respectively [30], as shown in Fig. 4(a). The even-symmetry dispersion-edge (DE) laser mode with a wavelength of 1549.6 nm and the odd-symmetry guided modes are unambiguously identified in Fig. 4(a). The incomplete suppression of the x-polarization of the DE mode is due to the fabrication imperfection of the air holes along the PhC waveguide and the large numerical aperture of the objective lens. The spectral distance between the even- and odd-symmetry guided modes agrees with the calculation result of Fig. 2(a). In comparison, with CNB on the identical PhC waveguide, a new resonant mode is generated from the even-symmetry dispersion-edge mode. From this CNB printed sample, single-mode lasing is observed at 1552.0 nm as shown in Fig. 4(b). The introduction of the CNB causes a red-shift by ~2.4 nm from the even-symmetry dispersion-edge mode. One can directly observe the EBID PhC mode and other even-symmetry guided modes simultaneously, by pumping an area with a diameter of ~8 μm which is much larger than the CNB region, as shown in Fig. 4(c). Through this experiment we confirm that the EBID PhC laser mode exists at a spectral position red-shifted from the cutoff of the original PhC waveguide (the dotted line of Fig. 4(c)).

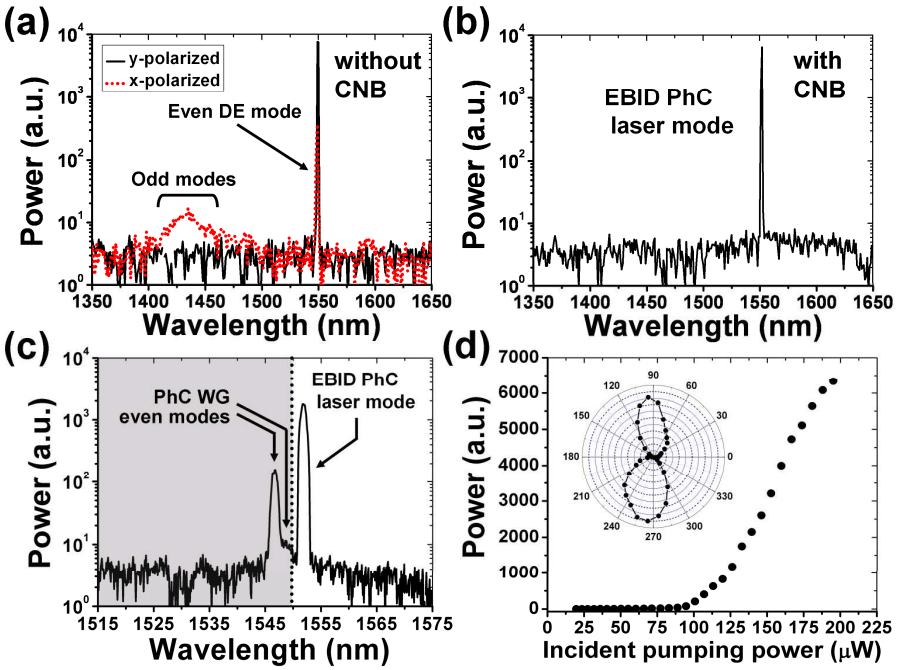

Fig. 4. (a) Polarization-resolved PL spectra of the PhC waveguide without CNB, with pump power of ~460 μW. The even-symmetry dispersion-edge laser mode is observed at a wavelength of 1549.6 nm. (b) EBID PhC laser lasing at 1552.0 nm. The spectrum is measured at an incident pumping level of ~270 μW. (c) Lasing spectra of showing both the EBID PhC laser and other even-symmetry guided modes. The pump area is increased to ~8 μm, in order to cover a wide area. The dotted line indicates the even-symmetry dispersion-edge (1549.6 nm) found in Fig. 4(a). (d) Light-in versus light-out curve and polarization characteristics of the EBID PhC laser of Fig. 4(b).

The threshold of the EBID PhC laser is ~100 μW as shown in the light-in versus light-out (L-L) curve (Fig. 4(d)). The L-L curve is plotted as a function of the incident peak pump power. The experimental Q factor is estimated from the full-width at half-maximum (FWHM) of the resonant mode under near-transparency conditions. The FWHM measured with pumping power of 0.8 times threshold is spectrometer-limited to ~0.5 nm which corresponds

#107040 - $15.00 USD Received 2 Feb 2009; revised 26 Mar 2009; accepted 6 Apr 2009; published 9 Apr 2009

to a Q factor of ~3000. On the other hand, the theoretical Q factor is computed to ~7000 (Figs. 2(d) and 2(e)) when the wavelength-shift of the mode is ~2.4 nm (Figs. 4(a) and 4(b)). Then, the absorption loss of the CNB can be estimated from the comparison of these theoretical and experimental Q factors. The upper bound of the absorption loss by the CNB is estimated to be ~7.7 cm^{-1} [32]. The laser output is linearly polarized along the direction orthogonal to the PhC waveguide axis (inset of Fig. 4(d)). This observation is another evidence that the EBID PhC laser mode originates from the even-symmetry dispersion-edge mode.

5. Effects of the nano-block position on Q factors and light emission

The Q factor of an EBID PhC cavity mode depends strongly on the position of the nano-block [34]. In Fig. 5(a), a CNB is deposited at the position shifted one half of the PhC lattice in comparison to the EBID PhC laser of Fig. 1(c). In this case, the nano-block is located at the node of the electric field intensity and does not generate an electric dipole moment effectively. Therefore, the vertical emission loss is reduced and Q factors, as shown in Fig. 5(d), are >10 times higher than those of the case with a nano-block at the position above the electric field maximum (Fig. 2(d)). The amount of the reduced vertical emitting loss becomes comparable to that of the optical loss to the PhC waveguide. In the near-field image at an above threshold (Fig. 5(c)), we can observe emission from the cavity region and also scattering of the photons leaking through the waveguide at the ends of the waveguide. Note that, in the EBID PhC cavity with a CNB above the electric field maximum, most of the photons are emitted at the cavity region to the vertical direction. In addition, the calculated cutoff wavelength shifts of the EBID PhC cavity with the CNB at the electric field node (Fig. 5(e)) are smaller than those of the EBID PhC cavity of Fig. 2(e). We expect that, by varying the position and size of the CNB, modal properties of the EBID PhC cavity mode, such as Q factors and emission output coupling, can be adjusted to the purposes of applications.

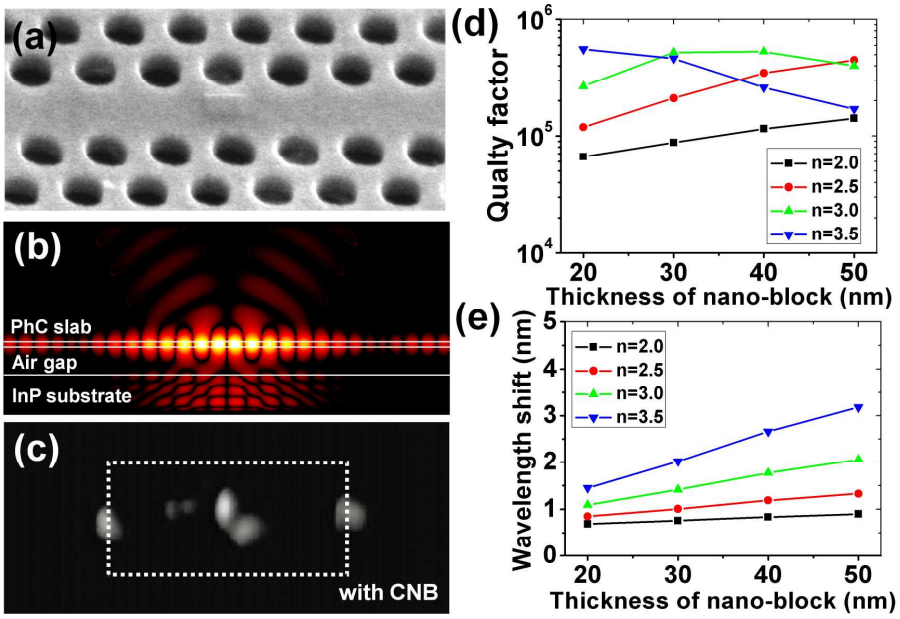

Fig. 5. (a) An EBID PhC laser with a CNB located at the node of electric field intensity. (b) Calculated side view of electric field intensity profile (log scale). (c) Near-field images of the EBID PhC laser in Fig. 5(a). Calculated Q factor (d) and cutoff wavelength-shift with various thicknesses and refractive indices of the CNB, when the CNB is created at the node of electric field intensity.

#107040 - $15.00 USD Received 2 Feb 2009; revised 26 Mar 2009; accepted 6 Apr 2009; published 9 Apr 2009

Figure 6 shows the lasing spectra measured in the PhC waveguide structures of Fig. 5(a). In the EBID PhC laser with the CNB, the resonant wavelength is red-shifted by ~2.2 nm from the even-symmetry dispersion-edge mode. This wavelength-shift is slightly smaller than the result from Figs. 4(a) and 4(b). In addition, as shown in Fig. 6(b), the CNB effectively suppresses the side odd- and even-symmetry guided modes observed in the PhC waveguide without the CNB of Fig. 6(a).

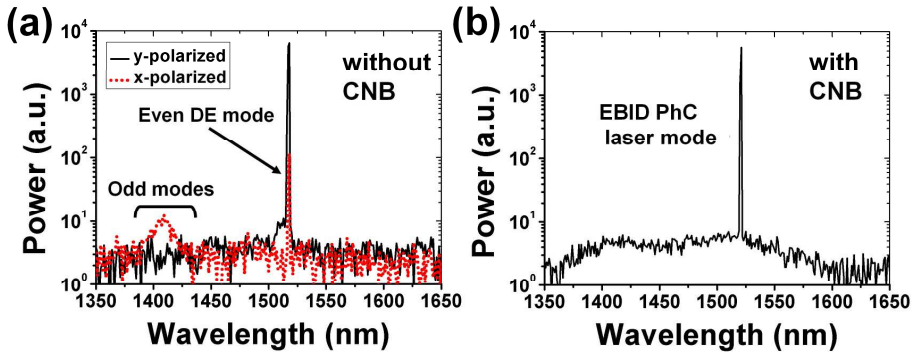

Fig. 6. (a) Polarization-resolved PL spectra of the PhC waveguide without CNB, with pump power of ~410 μW. The even-symmetry dispersion-edge laser mode is observed at a wavelength of 1518.4 nm. (b) EBID PhC laser with a CNB at the node of electric field intensity. The EBID PhC laser operates at 1520.6 nm. The spectrum is measured at an incident pumping level of ~270 μW.

6. Summary

The EBID wavelength-scale PhC laser is demonstrated using EBID techniques. This EBID PhC laser operates in a single mode with threshold of ~100 μW at room temperature. In addition, we measured the near-field profile and the polarization states of the EBID PhC cavity mode. The FDTD computation supports that a wavelength-scale cavity with a mode volume of ~1.4 $(\lambda/n)^3$ is well defined by a CNB in the PhC waveguide. We believe that the successful demonstration of the EBID PhC resonator represents a meaningful step in the field of nanophotonics and optical integrated circuits.

Acknowledgments

This work was supported by the Korea Science and Engineering Foundation (KOSEF) (No.ROA-2006-000-10236-0) and the Korea Foundation for International Cooperation of Science and Technology (KICOS) (No. M60605000007-06A0500-00710) through grants provided by the Korean Ministry of Science and Technology (MOST). H.G.P. acknowledges support by a Korea Research Foundation Grant funded by the Korean Government (KRF-2008-331-C00118) and the Seoul R&BD Program.